Korean J. Chem. Eng., 35(11), 2185-2190 (2018)
DOI: 10.1007/s11814-018-0135-4

pISSN: 0256-1115
eISSN: 1975-7220

Oxychlorination of methane over FeO_x/CeO_2 catalysts

Jeongeun Kim*, Youngseok Ryou*, Gyohyun Hwang, Jungup Bang**, Jongwook Jung**, Yongju Bang**, and Do Heui Kim*,†**

*School of Chemical and Biological Engineering, Institute of Chemical Processes, Seoul National University, 1 Gwanak-ro, Gwanak-gu, Seoul 08826, Korea
**Corporate R&D, LG Chem R&D Campus Daejeon, Ltd., 188 Munji-ro, Yuseong-gu, Daejeon 34122, Korea
(*Received 29 May 2018 • accepted 26 July 2018*)

Abstract−Methane activation through oxychlorination is in the spotlight due to the relatively mild reaction conditions at atmospheric pressure and in the temperature range of 450-550 °C. Although CeO_2 is known to exhibit good activity for methane oxychlorination, significant amounts of by-products such as CO_2, CO and carbon deposits are produced during the reaction over CeO_2. We investigated the effect of iron in FeO_x/CeO_2 catalysts on methane oxychlorination. FeO_x/CeO_2 with 3 wt% iron shows the maximum yield at 510 °C with 23% conversion of methane and 65% selectivity of chloromethane. XRD and H_2 TPR results indicate that iron-cerium solid solution was formed, resulting in the production of more easily reduced cerium oxide and the suppression of catalysts sintering during the reaction. Furthermore, the selectivity of by-products decreased more significantly over FeO_x/CeO_2 than cerium oxide, which can be attributed to the facilitation of HCl oxidation arising from the enhanced reducibility of the former sample.

Keywords: Methane, Oxychlorination, FeO_x/CeO_2, Reducibility of Surface Cerium, Chloromethane

INTRODUCTION

Methane is the main component of natural gas, which is regarded as an attractive chemical feedstock due to its abundance and low price. However, only under 10% of natural gas is currently used for chemical production, whereas 90% is just burned as fuel [1,2]. Therefore, the efficient conversion of methane to valuable chemicals has been considered important in the catalysis community. Nevertheless, methane activation remains as a challenging issue because methane has four highly stable C-H bonds (ΔH_d=439.3 kJmol^{-1}) [3], and any products from the conversion of methane have higher reactivity than methane [2,4]. Recently, commercialized methane activation processes such as steam reforming, partial oxidation and auto-thermal reforming are capital- and energy-intensive [1,2]. Although there are other methods to activate methane, for instance, CO_2 reforming, OCM (oxidative coupling of methane) and catalytic methane aromatization etc., process costs and product yields do not reach economical standard to be commercialized.

Hydrocarbon activation using halogen source has received the attraction from the viewpoint of the mild reaction condition in the range of 450-550 °C [2,4-11]. In addition, methyl halides, the products of the methane halogenation process, can be used as platform materials for various valuable chemicals [12]. Theoretically, methane halogenation with gaseous halogen occurs in the following reactions (1) and (2).

$$CH_4+Br_2\rightarrow CH_3Br+HBr,\ (\Delta H_r^o(298\ K)=-27.597\ kJmol^{-1}) \quad (1)$$

$$CH_4+Cl_2\rightarrow CH_3Cl+HCl,\ (\Delta H_r^o(298\ K)=-101.18\ kJmol^{-1}) \quad (2)$$

†To whom correspondence should be addressed.
E-mail: dohkim@snu.ac.kr

Bromine and chlorine are generally used as halogen source [2,12-16] due to the eruptive reactivity of fluorine and the excessive stability of iodide [2,13]. These reactions require the recovery step of X_2 from produced HX. On the other hand, methane oxidative halogenation as described in reactions (3) and (4) is thermodynamically more favorable than methane gaseous halogenation and, moreover, it does not require the recovery step [17].

$$CH_4+HBr+1/2O_2\rightarrow CH_3Br+H_2O,\ (\Delta H_r^o(298\ K)=-165.71\ kJmol^{-1}) \quad (3)$$

$$CH_4+HCl+1/2O_2\rightarrow CH_3Cl+H_2O,\ (\Delta H_r^o(298\ K)=-158.38\ kJmol^{-1}) \quad (4)$$

Various catalysts have been studied for the methane oxychlorination (metal oxychloride, metal phosphate etc.) [13]. Among them, cerium oxide has received attention recently [17,18]. The activity of cerium oxide is explained by the redox property of Ce^{4+}/Ce^{3+} which plays an important role in the oxidation of HCl to produce active Cl species for methane conversion [13,17-22]. Despite outstanding activity of cerium oxide, CO and CO_2 are produced as unwanted products of side reaction, resulting in a loss in carbon balance. Therefore, it is necessary to find a way to suppress the side reaction. In this study, various amounts of iron were introduced into cerium oxide to reduce the production of by-products (CO and CO_2) and increase the selectivity of chlorinated products. In addition, the effects of iron on lattice structure and redox property of cerium oxide were investigated to explain the excellent activity of FeO_x/CeO_2.

EXPERIMENTAL

1. Catalysts Preparation

FeO_x/CeO_2 catalysts with different iron loading were prepared by applying wet impregnation method. CeO_2 (Rhodia) was stirred

for 1 h in an aqueous solution of $Fe(NO_3)_3 \cdot 9H_2O$ (Sigma Aldrich), followed by the removal of the solvent by using a rotary evaporator. All catalysts were calcined in a muffle furnace at 600 °C for 6 h after drying at 100 °C overnight. The prepared catalysts are denoted as $FeO_x(x)/CeO_2$, which represents x wt% of iron loading.

2. Catalysts Characterization

X-ray photoelectron spectroscopy (XPS) analysis was conducted using K-alpha (Thermo VG, U.K.) with a AlKα X-ray source ($h\nu$= 1,486.6 eV). The spectra were corrected by using binding energy of C 1s (284.6 eV) [23,24].

The specific surface area of catalysts was determined by N_2 adsorption-desorption isotherm (Micromeritics ASAP 2010). For the measurement, the samples were evacuated at 250 °C for at least 5 h. The specific surface area was calculated by using Brunauer-Emmett-Teller (BET) method.

X-ray diffraction (XRD) patterns of the catalysts were taken with Ultra X18 (Rigaku Corp.) at 40 kV and 30 mA. Cu Kα was used as a radiation sources. All patterns were collected over 5-90° (2θ) with the scanning step size of 0.02°. The crystallite size was calculated by using Debye-Scherrer equation.

Transmission electron microscope (TEM) images captured by using JEM2100F (TEM, JEOL., Japan) were used to analyze the particles in the samples. Accelerating voltage for analysis is 200 kV.

H_2 temperature programmed reduction (H_2 TPR) analysis was carried out on a BEL CAT II (MicrotracBEL Corp.). The catalysts were pretreated at 400 °C for 1 h under air condition. After cooling to 40 °C, the catalysts were reduced with 5% H_2/Ar while increasing at 10 °C/min to 900 °C.

3. Catalytic Test

Methane oxychlorination was performed in a fixed bed quartz tubular reactor at atmospheric pressure. The 0.1 g catalyst, sieved in 0.18-0.25 mm, was tested from 450 to 550 °C and the reaction temperature was controlled by a thermocouple placed above the catalyst bed. Total inlet flow rate including reactants (CH_4, O_2, HCl), diluent (Ar) and internal standard (N_2) was controlled to 50 ml/min with the volume ratio of $CH_4 : O_2 : HCl : Ar : N_2$=4 : 1 : 2 : 3 : 10. Outlet stream was heated at 150 °C to avoid the condensation of the products and analyzed by using online gas chromatograph (Agilent Technologies 6890N/G1530N) with Carboxen 1000 packed column and HP Plot-Q capillary column. TCD (Thermal conductivity detector) and FID (Flame ionization detector) were used to analyze CH_4, O_2, N_2, CO_2 and CO, and CH_4, CH_3Cl (Chloromethane; CM), CH_2Cl_2 (Dichloromethane; DCM), and $CHCl_3$ (Trichloromethane; TCM), respectively. The oxidative chlorination of methane proceeds with change of mole number in reaction (4). Therefore, all GC data should be calibrated by using internal standard factor, α (Eq. (5)), where $n(N_2)$ is the amount of N_2 in moles.

$$\alpha = \frac{n(N_2)^{inlet}}{n(N_2)^{outlet}} \quad (5)$$

The conversion(X) of methane was determined by Eq. (6), where $n(CH_4)$ is the amount methane in moles.

$$X(CH_4) = \frac{n(CH_4)^{inlet} - \alpha \times n(CH_4)^{outlet}}{n(CH_4)^{inlet}} \times 100, \% \quad (6)$$

The selectivity (S) and yield (Y) for products were obtained from carbon basis by using Eq. (7) and Eq. (8), respectively, where n(j) is the amount of j component in moles (j denotes CM, DCM, TCM, CO or CO_2) [17].

$$S(j) = \frac{n(j)^{outlet}}{\Sigma n(j)^{outlet}} \times 100, \% \quad (7)$$

$$Y(j) = X(CH_4) \times S(j), \% \quad (8)$$

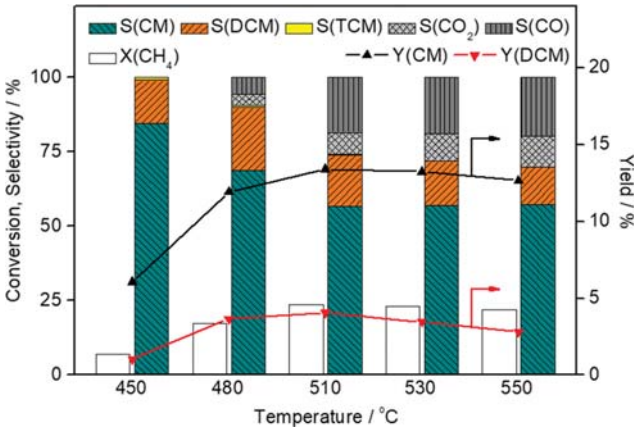

Fig. 1. Performance of CeO_2 for methane oxychlorination.

RESULTS AND DISCUSSION

1. Catalytic Properties for Methane Oxychlorination

The activity of cerium oxide for methane oxychlorination as a function of reaction temperature is shown in Fig. 1. Chlorinated products (CM, DCM and TCM) and by-products (CO and CO_2) are produced during the reaction. The selectivity of CM at 450 °C is 84.6% and decreases with an increment of reaction temperature. On the other hand, the selectivity of DCM is maximized at 480 °C as 21.1% and the selectivity of by-products (CO and CO_2) increases gradually with temperature. It is understood that the generated CM is further chlorinated and the chlorinated products are decomposed into CO or CO_2 during methane oxychlorination [25]. Similarly, the additional reaction of CM to multi-substituted materials by chlorine is facilitated with increasing temperature on cerium oxide. In addition, the decomposition of chlorinated products to CO and CO_2 is observed above 480 °C, resulting in the maximum selectivity of DCM at that temperature. According to the trade-off relationship between conversion and selectivity, the yield of chlorinated products is maximized at 510 °C with methane conversion of 23.6%, and the selectivity of 56.8% for CM and 17.2% for DCM. At the same time, the selectivity of CO and CO_2 is obtained as 18.5% and 7.2%, respectively. Taking into account the methane concentration of the reactants, the current results are similar to previous ones [17].

Fig. 2 shows the activity of $FeO_x(x)/CeO_2$ at 510 °C, where the yield of chlorinated products is maximized on cerium oxide as shown in Fig. 1. It seems that there is no advantage with the introduction of iron to cerium oxide from the viewpoint of methane conversion. However, the selectivity of by-products (CO and CO_2) is significantly reduced at comparable methane conversion. In par-

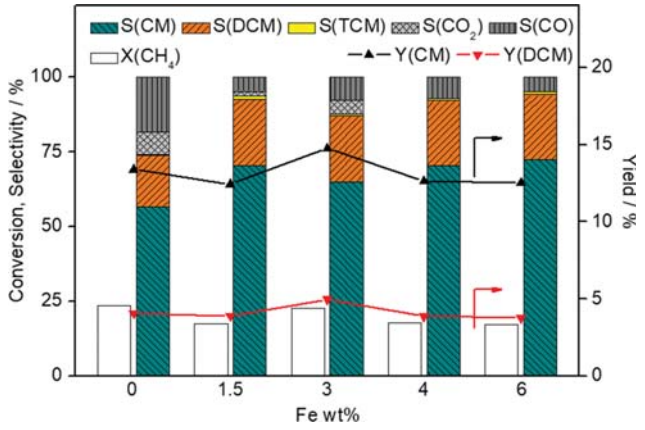

Fig. 2. Performance of FeO_x(x)/CeO_2 for methane oxychlorination at 510 °C.

ticular, no CO_2 is generated on FeO_x(4)/CeO_2 and FeO_x(6)/CeO_2. As a result, the selectivity of chlorinated products increases with the addition of iron regardless of iron loading amounts. The chlorinated products show the highest yield of about 20.0% over FeO_x(3)/CeO_2, with CM selectivity of 65.2% and DCM selectivity of 22.0%. In this case, the selectivity of CO and CO_2 are obtained as 7.8% and 4.6%, respectively, whereas those are attained as 18.5% and 7.2% over cerium oxide at the same temperature. It can be summarized that the addition of iron to cerium oxide gives rise to the increasing selectivity of chlorinated products by inhibiting the production of CO and CO_2.

2. Catalysts Characterization

X-ray photoelectron spectra for CeO_2 and FeO_x(3)/CeO_2 catalyst are shown in Figs. 3 and 4. In Fig. 3, three pairs of peaks in Ce 3d spectra labeled as v/u, v″/u″, and v‴/u‴ are arising from Ce^{4+} contributions and v′/u′ from Ce^{3+}, respectively [26]. There are no significant differences between fresh and used samples of FeO_x(3)/CeO_2 in Ce 3d photoelectron spectra. As shown in Fig. 4(a), the Auger peaks of cerium, which presents dominantly in the FeO_x/

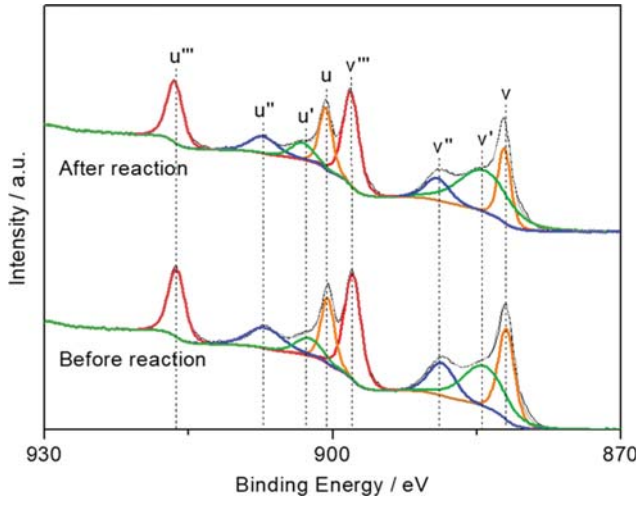

Fig. 3. XP spectra for Ce 3d of FeO_x(3)/CeO_2 before and after reaction.

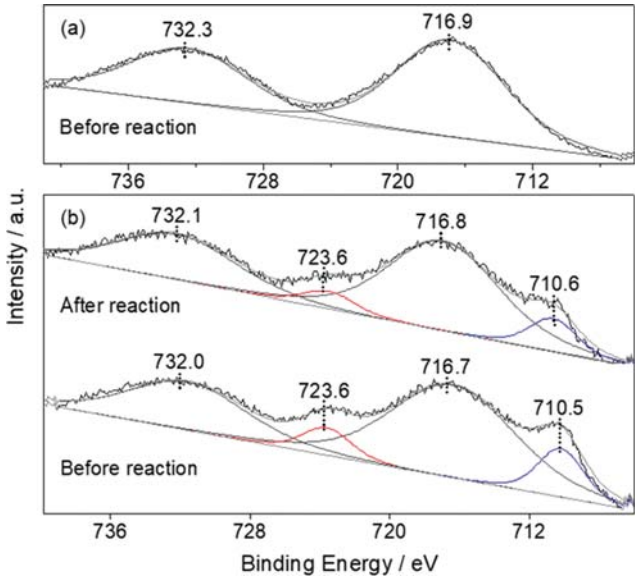

Fig. 4. XP spectra in Fe 2p region of (a) CeO_2 and (b) FeO_x(3)/CeO_2.

CeO_2, are obtained at 716.9 eV and 732.3 eV near the binding energy of Fe 2p satellite peaks [24,27]. Therefore, satellite peaks of Fe 2p, which overlap with the Auger peaks of cerium, are not clearly distinguished in Fig. 4(b). The peaks located at 710.6 eV and 723.6 eV are assigned to the main Fe $2p_{3/2}$ and Fe $2p_{1/2}$ of Fe^{3+}, respectively [27-31]. The intensity of the main Fe 2p peaks decreases after reaction, indicating that the relative surface concentration of iron in the catalyst is reduced.

The textural properties of fresh and used catalysts are summarized in Table 1. The surface area of fresh samples decreases abruptly from 132 m^2/g to 89 m^2/g when 1.5 wt% of iron is loaded on the pure cerium oxide, whereas the effect of iron loading amount on the surface area is negligible. A decrease in surface area is observed after the reaction in all samples, although the largest change occurs in pure cerium oxide. Average crystallite size of cerium oxide phase in fresh and used samples was determined by using Scherrer's equation with the reflections of (1 1 1). The calculated crystallite sizes of fresh catalyst are 10.4 nm in CeO_2, while those in used catalysts are 17.4 nm. However, the difference in crystallite size before and after reaction decreases on FeO_x(x)/CeO_2, indicating that sintering in cerium oxide catalysts during the reaction is significantly

Table 1. Textural properties of the catalysts with different iron loading

Sample	BET area (m^2/g)		Crystallite size (nm)		a[a] (Å)
	Fresh	Used at 510 °C	Fresh	Used at 510 °C	
CeO_2	132	71	10.4	17.4	5.390
FeO_x(1.5)/CeO_2	89	53	10.0	13.4	5.366
FeO_x(3)/CeO_2	87	56	10.4	12.1	5.357
FeO_x(4)/CeO_2	80	55	10.1	12.4	5.358
FeO_x(6)/CeO_2	78	50	10.7	12.4	5.381

[a]Unit cell lattice parameter of cerium oxide

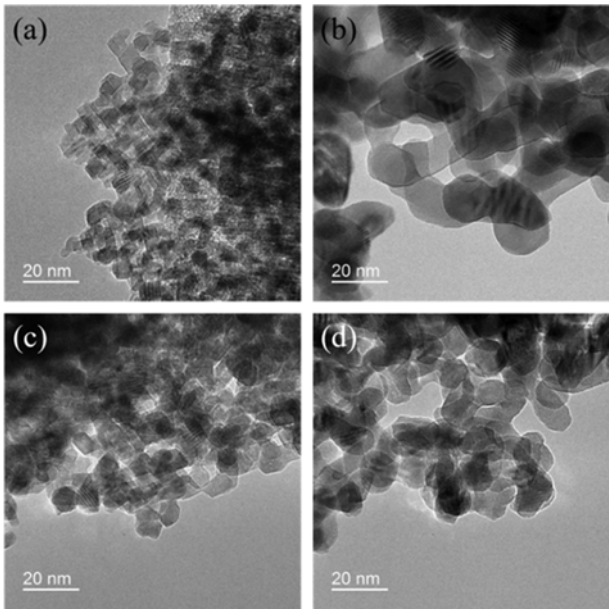

Fig. 5. TEM images of CeO_2 (a) fresh, (b) used at 510 °C and FeO_x/CeO_2 (c) fresh, (d) used at 510 °C.

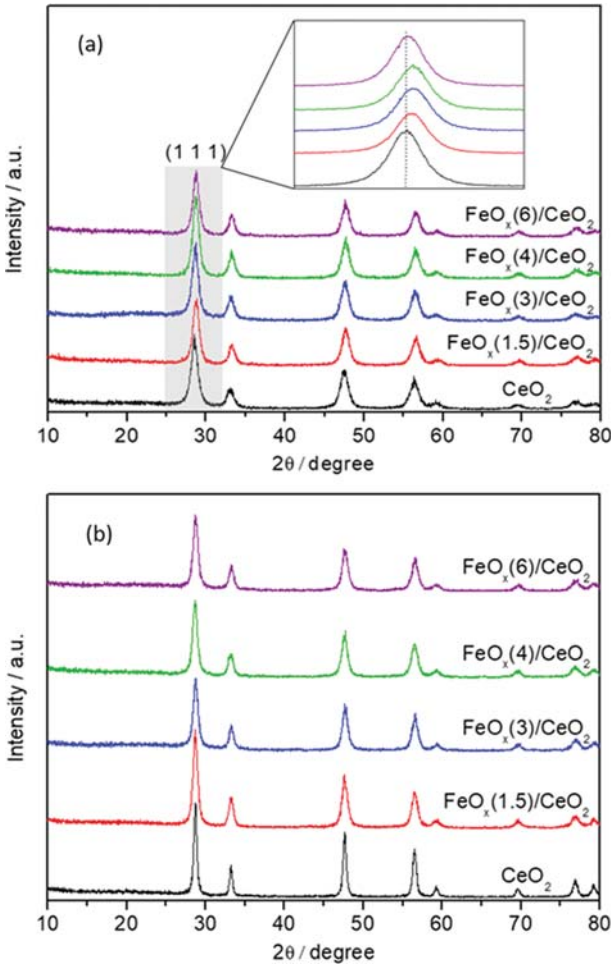

Fig. 6. XRD patterns of (a) fresh and (b) used at 510 °C catalysts with different iron loading.

suppressed with the addition of iron. Ceria-based average crystallite size in the samples was also measured by using TEM images of fresh and used samples (Fig. 5). The average crystallite size of CeO_2 is almost doubled from 9.4 nm to 17.8 nm after the reaction, although that of $FeO_x(3)/CeO_2$ increases slightly from 10.0 nm before the reaction to 12.7 nm after the reaction. These are consistent with XRD result.

Fig. 6 displays XRD patterns of fresh and used catalysts. The peaks in diffraction patterns of all samples are assigned to the cubic fluorite structure (JCPDS 34-0394, Fm3m) of cerium oxide [24,32, 33], and the structure is maintained after the reaction (Fig. 6(b)). The fact that no peaks matched with iron oxide phase were observed implies that solid solution of iron-cerium oxide is formed or that iron oxides are finely dispersed on cerium oxide. Additionally, the shift of cerium oxide (1 1 1) peak to higher angle in the box of Fig. 6(a) confirms the formation of iron-cerium solid solution [23]. As the iron content increases from 0 to 3 wt%, the (1 1 1) peak shift to higher angle and the corresponding unit cell lattice parameter decreases from 5.390 Å to 5.357 Å (Fig. 6(a), Table 1). The shrinkage of the unit cell occurs because small Fe^{3+} (0.64 Å) substitute large Ce^{4+} (1.01 Å) [23,24]. However, the difference in the unit cell lattice parameter between 3 and 4 wt% iron contents is negligible, implying that the iron concentration in the cerium oxide lattice reaches saturation point or that the solubility of iron to cerium is reduced due to the agglomeration of iron. The latter explanation is more persuasive, since the angle of (1 1 1) peak decreases and the unit cell lattice parameter increases with increasing of iron content from 4 to 6 wt%, indicating that the amount of iron forming the solid solution with cerium decreases. In summary, the degree of iron substitution in the cerium oxide cubic fluorite lattice is maximized when the iron content is 3 wt% and the addition of iron inhibits the sintering of the catalysts during methane oxychlorination.

H_2 TPR (H_2 temperature programmed reduction) was used to study the reducibility of the catalysts. It was reported that cerium oxide has two reduction steps at 300-600 °C and 700-1,000 °C, cor-

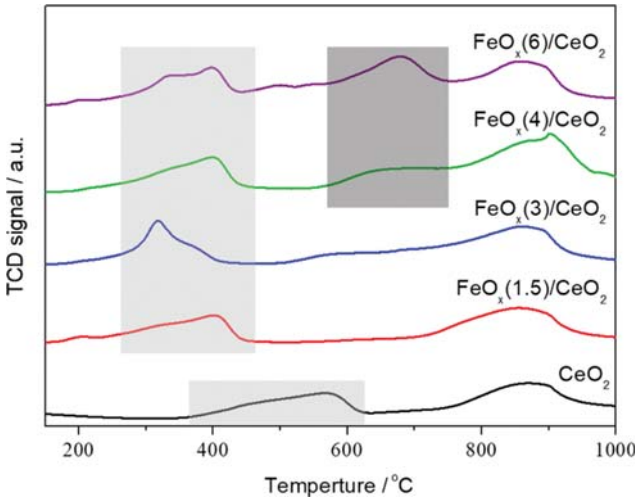

Fig. 7. H_2 TPR profiles of the fresh catalysts with different iron loading.

responding to the reduction of the surface and bulk cerium oxide, respectively [32,35]. In the case of iron oxide, there are three reduction steps at about 340 °C ($Fe_2O_3 \rightarrow Fe_3O_4$), 630 °C ($Fe_3O_4 \rightarrow FeO$) and 705 °C ($FeO \rightarrow Fe$) [23]. The H_2 TPR profiles of cerium oxide and $FeO_x(x)/CeO_2$ are shown in Fig. 7. The reduction peak of bulk cerium oxide in all samples was observed in the same temperature range (750 °C-950 °C). On the other hand, the position of peak corresponding to reduction of surface cerium oxide shifts to the lower temperature with the increasing of iron loading from 0 to 3 wt%. The peak shift can be explained by the fact that the concentration of oxygen vacancy in cerium oxide lattice increases by a charge compensating mechanism arising from the difference of oxidation number between Fe^{3+} and Ce^{4+} in Fe-Ce solid solution. In addition, the Ce-O bond is weakened with the introduction of the small amount of iron ions to cerium oxide [23,36-38]. However, the addition of the larger amount of iron than 3 wt% into cerium oxide rather reduces the reducibility of catalysts. This is because the iron forms coalesce, reducing the amount of Fe forming the solid solution with Ce (diminution of charge compensation mechanism) or occupy interstitial sites in the cubic fluorite lattice (interstitial compensation mechanism) blocking the oxygen vacancy sites, resulting in elimination of oxygen vacancy [23,38]. The agglomeration of iron is also confirmed by the reduction peaks at 600-750 °C observed in $FeO_x(4)/CeO_2$ and $FeO_x(6)/CeO_2$ which are assigned to the reduction peaks of Fe_3O_4 to Fe [23,39]. In summary, the highest surface reducibility of cerium oxide is observed over $FeO_x(3)/CeO_2$, where the maximum yield of chlorinated products is acquired, due to the increasing concentration of oxygen vacancy with Fe-Ce solid solution formation.

The order of elementary reaction rate in oxychlorination over cerium oxide is known to be HCl oxidation>methane chlorination> DCM and methane oxidation [17]. Accordingly, the rate of CM consumption via further chlorination or oxidation is considerably lower than the rate of CM production. Moreover, the reduced O_2 concentration arising from the fast HCl oxidation suppresses the further oxidation of CM [17], and thus, cerium oxide shows high selectivity of CM [13,17,18]. Since the most energy-demanding step in HCl oxidation is the activation of Cl atom, which is controlled by the redox cycle of cerium [19,21], the reducibility of surface cerium plays a key role in HCl activation [13,18]. Therefore, it can be proposed that the increased reducibility of cerium oxide by introducing iron facilitates the HCl oxidation step, thereby further enhancing the difference in the elementary reaction rate (HCl oxidation>methane chlorination>DCM and methane oxidation) and in CM production and consumption rate. As a result, the oxygen concentration in the reactant is further reduced and the further oxidation of CM or DCM is suppressed, resulting in the higher CM selectivity and the lower by-products (CO and CO_2) selectivity over FeO_x/CeO_2 than cerium oxide.

CONCLUSIONS

Methane oxychlorination was performed over $FeO_x(x)/CeO_2$ catalysts. The yield of CM was maximized at 510 °C where the methane conversion and CM selectivity were obtained as 23% and 65% over $FeO_x(3)/CeO_2$, respectively. The calculated crystallite size of cerium oxide phase in fresh and used catalysts implies that the iron suppresses the sintering of catalysts during methane oxychlorination with the formation of iron-cerium solid solution, which is confirmed by XRD and H_2 TPR results. In addition, the incorporated iron promotes the facile reduction of cerium oxide, especially on $FeO_x(3)/CeO_2$, resulting in the increased HCl oxidation rate. In conclusion, $FeO_x(3)/CeO_2$ demonstrates the highest yield of chlorinated products, which is explained by the increased reducibility of cerium oxide, attributed to the formation of iron-cerium solid solution.

ACKNOWLEDGEMENT

This work was supported by the LG Chem.

REFERENCES

1. V. Paunović, G. Zichittella, M. Moser, A. P. Amrute and J. Pérez-Ramírez, *Nat. Chem.*, **8**, 803 (2016).
2. R. Horn and R. Schlögl, *Catal. Lett.*, **145**, 23 (2015).
3. P. Schwach, X. Pan and X. Bao, *Chem. Rev.*, **117**, 8497 (2017).
4. E. Peringer, S. G. Podkolzin, M. E. Jones, R. Olindo and J. A. Lercher, *Top. Catal.*, **38**, 211 (2006).
5. Z. Li, G. Zhou, C. Li and T. Cheng, *Catal. Commun.*, **40**, 42 (2013).
6. C. Li, G. Zhou, L. Wang, Z. Li, Y. Xue and T. Cheng, *Catal. Commun.*, **13**, 22 (2011).
7. N. B. Muddada, T. Fuglerud, C. Lamberti and U. Olsbye, *Top. Catal.*, **57**, 741 (2014).
8. V. Paunović, G. Zichittella, S. Mitchell, R. Hauert and J. Pérez-Ramírez, *ACS Catal.*, **8**, 291 (2017).
9. V. Paunović, G. Zichittella, R. Verel, A. P. Amrute and J. Pérez-Ramírez, *Angew. Chem. Int. Ed.*, **55**, 15619 (2016).
10. V. Paunović, M. Artusi, R. Verel, F. Krumeich, R. Hauert and J. Pérez-Ramírez, *J. Catal.*, **363**, 69 (2018).
11. L. Xueju, L. Jie, Z. Guangdong, Z. Kaiji, L. Wenxing and C. Tiexin, *Catal. Lett.*, **100**, 153 (2005).
12. W. Taifan and J. Baltrusaitis, *Appl. Catal. B Environ.*, **198**, 525 (2016).
13. R. Lin, A. Amrute and J. Pérez-Ramírez, *Chem. Rev.*, **117**, 4182 (2017).
14. B. Wang, S. Albarracín-Suazo, Y. Pagán-Torres and E. Nikolla, *Catal. Today*, **285**, 147 (2017).
15. R. Lin, Y. Ding, L. Gong, J. Li, W. Chen, L. Yan and Y. Lu, *Appl. Catal. A Gen.*, **353**, 87 (2009).
16. V. Paunović, R. Lin, M. Scharfe, A. P. Amrute, S. Mitchell, R. Hauert and J. Pérez-Ramírez, *Angew. Chem. Int. Ed.*, **56**, 9923 (2017).
17. G. Zichittella, V. Paunović, A. P. Amrute and J. Pérez-Ramírez, *ACS Catal.*, **7**, 1805 (2017).
18. J. He, T. Xu, Z. Wang, Q. Zhang, W. Deng and Y. Wang, *Angew. Chem. Int. Ed.*, **51**, 2438 (2012).
19. A. P. Amrute, C. Mondelli, M. Moser, G. Novell-Leruth, N. López, D. Rosenthal, R. Farra, M. E. Schuster, D. Teschner and T. Schmidt, *J. Catal.*, **286**, 287 (2012).
20. A. P. Amrute, C. Mondelli, M. A. G. Hevia and J. Pérez-Ramírez, *ACS Catal.*, **1**, 583 (2011).
21. M. Capdevila-Cortada, G. Vilé, D. Teschner, J. Pérez-Ramírez and N. López, *Appl. Catal. B Environ.*, **197**, 299 (2016).

22. C. Li, Y. Sun, I. Djerdj, P. Voepel, C.-C. Sack, T. Weller, R. d. Ellinghaus, J. Sann, Y. Guo and B. M. Smarsly, *ACS Catal.*, **7**, 6453 (2017).
23. W. Wang, Q. Zhu, F. Qin, Q. Dai and X. Wang, *Chem. Eng. J.*, **333**, 226 (2018).
24. A. S. Reddy, C.-Y. Chen, C.-C. Chen, S.-H. Chien, C.-J. Lin, K.-H. Lin, C.-L. Chen and S.-C. Chang, *J. Mol. Catal. A Chem.*, **318**, 60 (2010).
25. S. G. Podkolzin, E. E. Stangland, M. E. Jones, E. Peringer and J. A. Lercher, *J. Am. Chem. Soc.*, **129**, 2569 (2007).
26. Y. Jiang, C. Bao, Q. Liu, G. Liang, M. Lu and S. Ma, *Catal. Commun.*, **103**, 96 (2018).
27. T. Yamashita and P. Hayes, *Appl. Surf. Sci.*, **254**, 2441 (2008).
28. P. Mills and J. Sullivan, *J. Phys. D Appl. Phys.*, **16**, 723 (1983).
29. P. C. Graat and M. A. Somers, *Appl. Surf. Sci.*, **100**, 36 (1996).
30. S. Roosendaal, B. Van Asselen, J. Elsenaar, A. Vredenberg and F. Habraken, *Surf. Sci.*, **442**, 329 (1999).
31. Thermo Fisher Scientific Inc., http://xpssimplified.com/elements/iron,php (accessed 22 January 2018).
32. M. F. Mohamad, A. Ramli and S. Yusup, *AIP Conf. Proc.*, **1502**, 288 (2012).
33. Z. Cui, J. Fan, H. Duan, J. Zhang, Y. Xue and Y. Tan, *Korean J. Chem. Eng.*, **34**, 29 (2017).
34. F. Pérez-Alonso, M. López Granados, M. Ojeda, P. Terreros, S. Rojas, T. Herranz, J. Fierro, M. Gracia and J. Gancedo, *Chem. Mater.*, **17**, 2329 (2005).
35. Y. Li, B. Zhang, X. Tang, Y. Xu and W. Shen, *Catal. Commun.*, **7**, 380 (2006).
36. A. Trovarelli, *Commun. Inorg. Chem.*, **20**, 263 (1999).
37. L. Kongzhai, W. Hua, W. Yonggang and L. Mingchun, *J. Rare Earths*, **26**, 245 (2008).
38. W. Cai, F. Chen, X. Shen, L. Chen and J. Zhang, *Appl. Catal. B Environ.*, **101**, 160 (2010).
39. L. Tang, D. Yamaguchi, N. Burke, D. Trimm and K. Chiang, *Catal. Commun.*, **11**, 1215 (2010).